Astron. Astrophys. 299, 545–556 (1995)

ASTRONOMY
AND
ASTROPHYSICS

Frequency dependent radiation transfer in protostellar disks

C. Sonnhalter, Th. Preibisch, and H.W. Yorke

Astronomisches Institut der Universität Würzburg, Am Hubland, D-97074 Würzburg, Germany,
Internet: cordula@astro.uni-wuerzburg.de; yorke@astro.uni-wuerzburg.de; preib@astro.uni-wuerzburg.de

Received 27 July 1994 / Accepted 13 December 1994

Abstract. The distributions of dust temperatures and mean radiation intensities in axially symmetric dusty disks are calculated within the framework of the flux-limited diffusion approximation. A multi-component dust model, consisting of amorphous carbon and silicate grains, which are coated with "dirty ice", is employed. After determination of the dust temperatures a ray-tracing procedure is used to calculate the spectral appearance of the disk at varying inclinations and to produce isophote maps at selected frequencies. The spatial distribution of dust temperatures resulting from these calculations reflect the shape of a disk's density distribution and do not display a simple (distance)$^{-a}$ power law. The spectra calculated from the same disk model at different inclinations can vary over a wide range. It is therefore often not possible to derive parameters of a disk — in particular its evolutionary state — from the spectrum alone. It is not recommended to infer the existence of planets by using simple temperature power law fits to disk spectra in combination with simple power law dust opacities.

Key words: radiation transfer – stars: circumstellar matter – stars: formation of

1. Introduction

The transfer of radiation in dusty molecular clumps plays a key rôle in the star formation process. On the one hand, the temperature and composition and thus the thermodynamics of both the dust and gas depend on the local radiation field. On the other hand, pressure effects and radiative acceleration influence the hydrodynamic evolution of the clump. Numerical modeling of these processes and the detailed interpretation of observations depend crucially on the application of adequate methods of solution of the radiation transfer problem.

The radiation field is described by the 6-D phase space density of photons, which is proportional to the radiation intensity I_ν at a point x and frequency ν in a line of sight in direction $\hat{s}$ (x represents the three space dimensions, ν and $\hat{s}$ the three momentum variables). Because the evolution of molecular clumps is invariably a time-dependent problem — the state of a molecular cloud is intimately related to its previous history — the mathematical description of the radiation field requires seven independent variables. In order to keep this problem numerically tractable simplifying assumptions have to be made. Symmetry considerations and use of the "grey approximation" are the most common of such simplifications.

For many years it has been possible to solve frequency dependent continuum radiation transfer simultaneously with the hydrodynamic problem under the assumption of spherical symmetry (Yorke 1979; Yorke 1980a; Yorke 1980b). Because, however, the formation of circumstellar disks is a natural consequence of the star formation process (Strom et al. 1993; Beckwith & Sargent 1993) and collimated outflows commonly occur in newly formed star/disk systems (Palla 1993; Zinnecker et al. 1992), a realistic description of the the star formation problem involves radiation transfer with at most axial symmetry. Efstathiou & Rowan-Robinson (1990) describe an exact code for solving the radiation transfer problem in axial symmetry, but their numerical resolution is extremely low and the computational effort appears to be huge, since only a few calculations with this code have been published.

A more common approach is the use of the grey diffusion approximation (e.g. Tscharnuter & Boss 1993; Boss 1987) or the grey flux-limited diffusion (hereafter FLD) approximation (Bodenheimer et al. 1990; Yorke et al. 1993; Yorke & Kaisig 1994) for the determination of dust temperatures, followed by a ray-tracing procedure, e.g. Yorke (1986), or a Monte-Carlo calculation (Fischer et al. 1994) for the determination of spectra and isophote maps (and polarization maps in the last example). Recently, Preibisch et al. (1994) have examined the validity of the grey approximation in dusty envelopes by comparison with exact 1D (spherically symmetric) and 2D (axially symmetric) frequency dependent calculations. The 2D problem was solved by the code presented and discussed here. Preibisch et al. (1994) conclude that the grey approximation is inadequate for dusty protostellar envelopes. With this result in mind we discuss the numerical solution of the frequency dependent FLD problem and present the results for several different axially symmetric density configurations.

Send offprint requests to: C. Sonnhalter

2. The radiation transfer problem

2.1. Basic equations

The change of radiation intensity $I_\nu(\boldsymbol{x}, \hat{\mathbf{s}})$ is determined by the equation of radiative transfer (together with boundary and initial conditions):

$$\frac{1}{c}\frac{\partial I_\nu}{\partial t} + \hat{\mathbf{s}} \cdot \nabla I_\nu = \sum_i \left(\kappa_\nu^{\mathrm{a}\,i} B_\nu(T_i) + \kappa_\nu^{\mathrm{s}\,i} J_\nu - \kappa_\nu^{\mathrm{e}\,i} I_\nu\right) \tag{1}$$

c is the speed of light, $\kappa_\nu^{\mathrm{a,e,s}^i}$ the *a*bsorption, *e*xtinction or *s*cattering coefficient of the ith dust component, T_i the corresponding dust temperature and B_ν Planck's function. Isotropic scattering is implicitly assumed. (1) is an integro-differential equation for I_ν, which in general must be solved iteratively, a very time and memory consuming affair. In general simplifications must be made such as the grey approximation or symmetry assumptions.

Instead of the transfer equation (1), its angular moment equations can be used. In their entirety they contain the same information as the transfer equation itself. However, the equation for the kth moment introduces $2k + 1$ new unknowns (the components of $k + 1$st moments); this system is complete only for an infinite number of moment equations. Numerical solutions are possible when a finite number of moment equations are used in conjunction with *closure* relations, which approximate the highest moments as a function of lower moments.

The zeroth moment equation is obtained by integrating the transfer equation over all solid angles Ω. Assuming isotropic, thermal dust emission, it can be written

$$\frac{1}{c}\frac{\partial J_\nu}{\partial t} + \nabla \cdot \boldsymbol{H}_\nu = \sum_i \kappa_\nu^{\mathrm{a}\,i} \left(B_\nu(T_i) - J_\nu\right), \tag{2}$$

where the zeroth and first moments J_ν and $\boldsymbol{H}_\nu$ are defined as

$$J_\nu = \frac{1}{4\pi}\int_\Omega I_\nu \,\mathrm{d}\Omega \quad \text{and} \quad \boldsymbol{H}_\nu = \frac{1}{4\pi}\int_\Omega I_\nu \hat{\mathbf{s}}\,\mathrm{d}\Omega. \tag{3}$$

J_ν is proportional to the radiative energy density $u_\nu = 4\pi/c\, J_\nu$ and $\boldsymbol{H}_\nu$ to the radiative flux $\boldsymbol{F}_\nu = 4\pi\, \boldsymbol{H}_\nu$.

Thus the moment equation can be solved for J_ν if there is a relation between flux and and energy density i.e. the zeroth and first moment. In fact, such a physical relation exists in two limiting cases: In vacuum the flux and the energy density of photons moving in a certain direction are related by $F_\nu = c\,u_\nu$ and in the optically thick case photons diffuse according to Fick's law, $\boldsymbol{F}_\nu = \mathscr{D}\, \nabla u_\nu$, where $\mathscr{D}$ is the diffusion coefficient of the material. There is no general relation, which connects these two quantities.

Assuming that I_ν/J_ν is a slowly varying function of space and time, Levermore & Pomraning (1981) derived the following approximate expression for such a closure relation from the transfer and zeroth moment equations and called it flux-limited diffusion (FLD):

$$\boldsymbol{H}_\nu = -\frac{\lambda_\nu}{\sum_i \kappa_\nu^{\mathrm{e}\,i}\omega_\nu}\nabla J_\nu. \tag{4}$$

The effective albedo ω_ν and the flux limiter λ_ν are defined as:

$$\omega_\nu = \sum_i \frac{\kappa_\nu^{\mathrm{a}\,i} B_\nu(T_i) + \kappa_\nu^{\mathrm{s}\,i} J_\nu}{\kappa_\nu^{\mathrm{e}\,i} J_\nu},$$

$$\lambda_\nu = \frac{1}{d}\left(\coth d - \frac{1}{d}\right) \quad \text{with} \quad d = \left|\frac{\nabla J_\nu}{\sum_i \kappa_\nu^{\mathrm{e}\,i}\omega J_\nu}\right|. \tag{5}$$

FLD gives the correct values in both of the limiting cases discussed above.

In a steady state a dust particle of species i should absorb and emit the same amount of total energy. If energy exchange via particle collisions can be neglected and isotropic thermal emission of the dust is assumed, then

$$\int_0^\infty \kappa_\nu^{\mathrm{a}\,i}\, B_\nu(T^i)\,\mathrm{d}\nu = \int_0^\infty \kappa_\nu^{\mathrm{a}\,i} J_\nu\,\mathrm{d}\nu. \tag{6}$$

This equation defines the dust temperature of component i. Note that the relation holds for a specific dust species and that dust grains of different composition or size will in general attain different dust temperatures in the same radiation field.

The moment equation (2) together with the closure relation from FLD (4) and the temperature equations for the dust components (6) comprise a self consistent description of continuum radiation transfer in the dusty disk.

2.2. The numerical model and method of solution

The following model configuration was examined. A central source is embedded in a dusty envelope, whose density distribution is axially symmetric with respect to the z-axis and mirror symmetric with respect to the plane $z = 0$ containing the central source. Cylindrical coordinates (z, r, ϕ) are used, because the symmetry now reduces the relevant information to the first quadrant of the r-z plane.

For a complete description of the problem, initial and boundary conditions have to be specified. It is assumed that the envelope is embedded in an external radiation field. The zeroth moment at the outer boundaries $\boldsymbol{x} = (z, r_{\max})$ and $\boldsymbol{x} = (z_{\max}, r)$ is fixed to be

$$J_\nu = B_\nu(T_{\mathrm{out}}) \quad \text{with} \quad T_i \equiv T_{\mathrm{out}} = 20\ \mathrm{K}. \tag{7}$$

At the inner boundaries, $z = 0$ and $r = 0$, the symmetry conditions must be satisfied.

$$\left.\frac{\partial J_\nu(z,r)}{\partial r}\right|_{r=0} = 0, \quad \left.\frac{\partial J_\nu(z,r)}{\partial z}\right|_{z=0} = 0. \tag{8}$$

The equations are discretized on a quadratic, equally spaced grid with spacing Δ. A grid point $\boldsymbol{x}_{k,j} = (z_k, r_j)$ is defined by $r_j = (j-1)\Delta$ and $z_k = (k-1)\Delta$. The quantities J_ν, $\kappa_\nu^{\mathrm{a}\,i}$, $\kappa_\nu^{\mathrm{e}\,i}$, the density ϱ and the dust temperatures T_i are defined at the center of a grid cell, e.g. $J_{\nu\,k,j} = J_\nu(z_k - \Delta/2, r_j - \Delta/2)$. Fluxes are defined at cell boundaries.

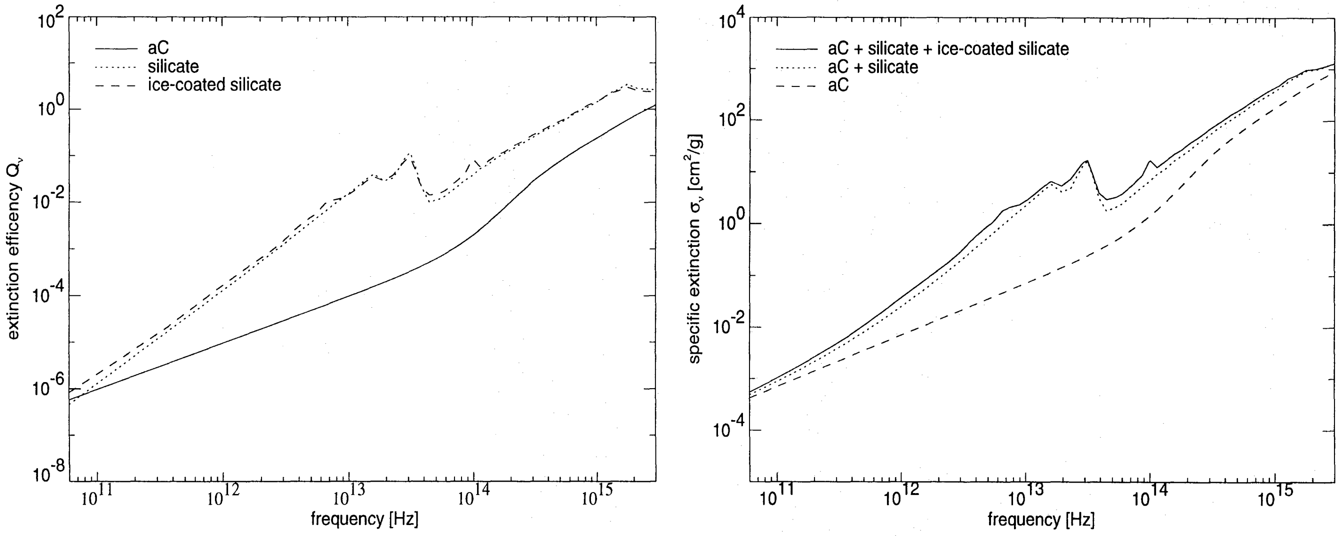

Fig. 1. Extinction efficiency and specific extinction between 2000 and 1500 K (aC), between 1500 and 125 K (aC + silicate) and below 125 K (aC + silicate + ice-coated silicate)

The emission from the central source is included as an additional emissivity ϵ^* in the innermost cell.

$$\epsilon_\nu^* = \frac{r_*^2}{2\Delta^3} B_\nu(T_*) \quad \text{with} \quad r_* = \sqrt{\frac{L_*}{4\pi\sigma T_*^4}}. \tag{9}$$

L_* is the total luminosity of the central source, T_* its temperature and r_* its radius.

To improve resolution and convergence, nested grids with $\Delta_{l+1} = \Delta_l/2$ are used (see Yorke & Kaisig 1994).

Substituting the expression for $\boldsymbol{H}_\nu$ given in Eq. (4) into Eq. (2) we obtain a system of 64 partial differential equations, which only depend on J_ν and T_i at each of the 64 frequencies considered. These elliptical type equations were solved using an *alternating direction implicit* (ADI) method (cf. Marsal 1976; Press et al. 1992). The differential equations for J_ν are iterated together with the temperature equations (6) until a self-consistent equilibrium configuration is reached. A more detailed description of the code can be found in Sonnhalter (1993).

2.3. The dust model

Knowledge of the absorption, extinction and scattering coefficients of the envelope's material are required. Except for line radiation, they are dominated by the optical properties of the dust. Assuming spherical dust grains, the absorption and scattering efficiencies $Q_\nu^{a,s}$ can be calculated using Mie theory. The optical coefficients then follow from

$$\kappa_\nu^i = \varrho\, \sigma_\nu^i \quad \text{with} \quad \sigma_\nu^i = G^i\, \pi \left\langle a^2 \right\rangle \langle Q_\nu \rangle\,. \tag{10}$$

G^i is the abundance of species i, i.e. the number of grains per unit mass, $\left\langle a^2 \right\rangle$ the mean squared radius of the grains and $\langle Q_\nu \rangle$ the radius averaged efficiency and ϱ the density.

We use a dust model from Preibisch et al. (1993), which models the dust properties in dense molecular clouds. It consists of small amorphous carbon (aC) and large silicate grains. It assumes that the silicate grains are coated with a mantle of "dirty ice" if their temperature is below 125 K. The radii a_i of the grains obey the following power law distribution:

$$n(a) \propto a^{-3.5} \qquad \text{for} \qquad a_{i,\min} \leq a \leq a_{i,\max}$$

where, in contrast to Mathis et al. (1977), we assume that the aC grain radii range from 7 nm to 30 nm, the silicate radii from 40 nm to 1 μm. The ratio between the radii of ice-coated and uncoated silicate grains is 1.145. The "dirty ice" consists of a 3:1 (volume) mixture of H_2O and NH_3, which is polluted with 10 % carbon particles. When the ice coatings sublimate, the aC particles are set free and a "naked" silicate grain remains. The sublimation temperatures of the silicate and aC particles are taken to be 1500 K and 2000 K. The extinction efficiency of the dust components and the specific extinction of the dust are shown in Fig. 1.

2.4. The density models

In addition to the dust composition a density distribution for the envelope has to be specified. We used a model configuration that is based on the distributions examined by Lazareff et al. (1990). It consists of three components that are smoothly switched on and off by Fermi-type functions: An analytical disk distribution $\varrho_{\rm disk}$ is embedded in a spherical halo, which has wind-blown cavities along the rotational axis. The total density can be written as

$$\begin{aligned} \varrho(z,r) \;=\; & \varrho_{\rm disk} \left(1 + e^{(r - r_{\rm s})/\alpha}\right)^{-1} \\ & + \varrho_{\rm halo} \left[\left(1 + e^{-(r - r_{\rm s})/\alpha}\right) \right. \\ & \left. \times \left(1 + e^{(z - z_{\rm h}) \cos\theta/\alpha}\right)\right]^{-1}. \end{aligned} \tag{11}$$

The parameters r_s and $z_s = h\, r_s$ fix radius and height of the disk. α determines the width of the transition zone of the Fermi-type functions. $\varrho_{\rm halo}$ is given by

$$\varrho_{\rm halo} = \varrho_s \frac{r_s^2}{r^2 + z^2}. \tag{12}$$

ϱ_s is the density of the disk at $r = r_s$ and $z = 0$. Points with $z > z_h$ lie within the cavities. They are modeled by

$$z_h = z_s \left(\frac{r}{r_s}\right)^4, \tag{13}$$

The slope of z_h fixes θ by

$$\cos\theta = \left(1 + \left(4\frac{z_h}{r}\right)^2\right)^{-1/2}. \tag{14}$$

For the density of the disk $\varrho_{\rm disk}$ several analytical distributions were employed:

The vertical structure of an isothermal, self gravitating disk can be approximated by an exponential, the radial distribution follows a power law with an exponent γ that depends on the rotation curve of the disk.

$$\varrho_{\rm disk}^{d1-d3} = \varrho_s \left(\frac{r_s}{r}\right)^\gamma e^{-z/(r\cdot h)}. \tag{15}$$

In model d1 the rotational velocity v_{rot} is constant and $\gamma = 2$. If v_{rot} is proportional to the square root of r, then $\gamma = 1$ (model d2). $\gamma = 0$, if the disk rotates like a rigid body as in model d3.

Simple model calculations often use an infinite, isothermal slab to approximate the disk around a young stellar object. Its density depends only on the distance from the equatorial plane.

$$\varrho_{\rm disk}^{d4} = \varrho_s e^{-z/z_s}. \tag{16}$$

If the central potential of the star is the dominating gravitational potential in the disk, a Keplerian disk is formed. For such a disk Shakura & Sunyaev (1973) calculated the following density distribution:

$$\varrho_{\rm disk}^{d5} = \varrho_s \left(\frac{r_s}{r}\right)^{15/8} e^{-\pi/4\left(z/z_s\,(r_s/r)^{9/8}\right)^2}. \tag{17}$$

3. Results

For a given density and dust model we can now study the frequency dependent radiation transport within the envelope. If the differential equations for the mean intensity ((2) combined with (4)) are solved together with the temperature equation (6), we get frequency dependent mean intensities and dust temperatures. In a second step a ray-tracing procedure (Yorke 1986) is used to calculate intensity maps at several wavelengths and the spectral distribution of the emitted flux. Table 1 summarizes the input parameters of the examined models.

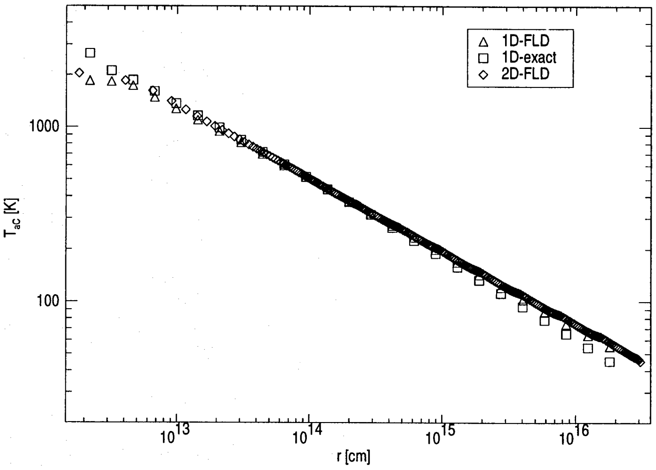

Fig. 2. Comparison of the results for a spherical symmetric density distribution using an exact 1D, the FLD 1D code and the FLD 2D code

Table 1. Parameters used in the calculations

density model	L_*	T_*	$T_{\rm out}$	$r_{\max} = z_{\max}$
d1 – d5	20 $L_\odot$	5000 K	20 K	$1.5 \cdot 10^{16}$ cm
ϱ_s	r_s	h	z_s	α
10^{-18} g cm^{-3}	10^{16} cm	0.25	$h\, r_s$	$0.1\, r_s$

3.1. Test calculations

We tested our 2D code and compared the results to two 1D calculations using the spherical symmetric density distribution

$$\varrho_{\rm test}(r) = \varrho_o \frac{1}{r} \quad \text{with} \quad \varrho_o = \frac{M}{2\pi R^2}, \tag{18}$$

where $M = 5 \cdot 10^{31}$ g and $R = 3.16 \cdot 10^{16}$ cm. The first 1D program solves the frequency dependent FLD equations in spherical symmetry (Preibisch 1992), the second calculates an exact solution of the equation of radiative transfer (1) (Yorke 1980b; Okorokov et al. 1985).

The principal advantage of the 1D programs is that they work with a logarithmically spaced r-grid. Thus, the innermost part of the envelope, where the density and temperature gradients are very large, can be resolved quite well using a reasonable number of grid points. In contrast, our 2D code is based on an equally spaced grid. In order to improve the spatial resolution near the center we introduced a series of nested grids. Still, we were not able to match the resolution of the logarithmically spaced grid with a reasonable amount of computational effort.

In Fig. 2 we compare the temperatures of the aC grains found with the three programs. The temperature distribution from our 2D program matches quite well the one from the 1D FLD program. The deviations at the innermost and outermost parts can be attributed entirely to the difference in resolution. Using a coarser grid in the central region leads to lower optical

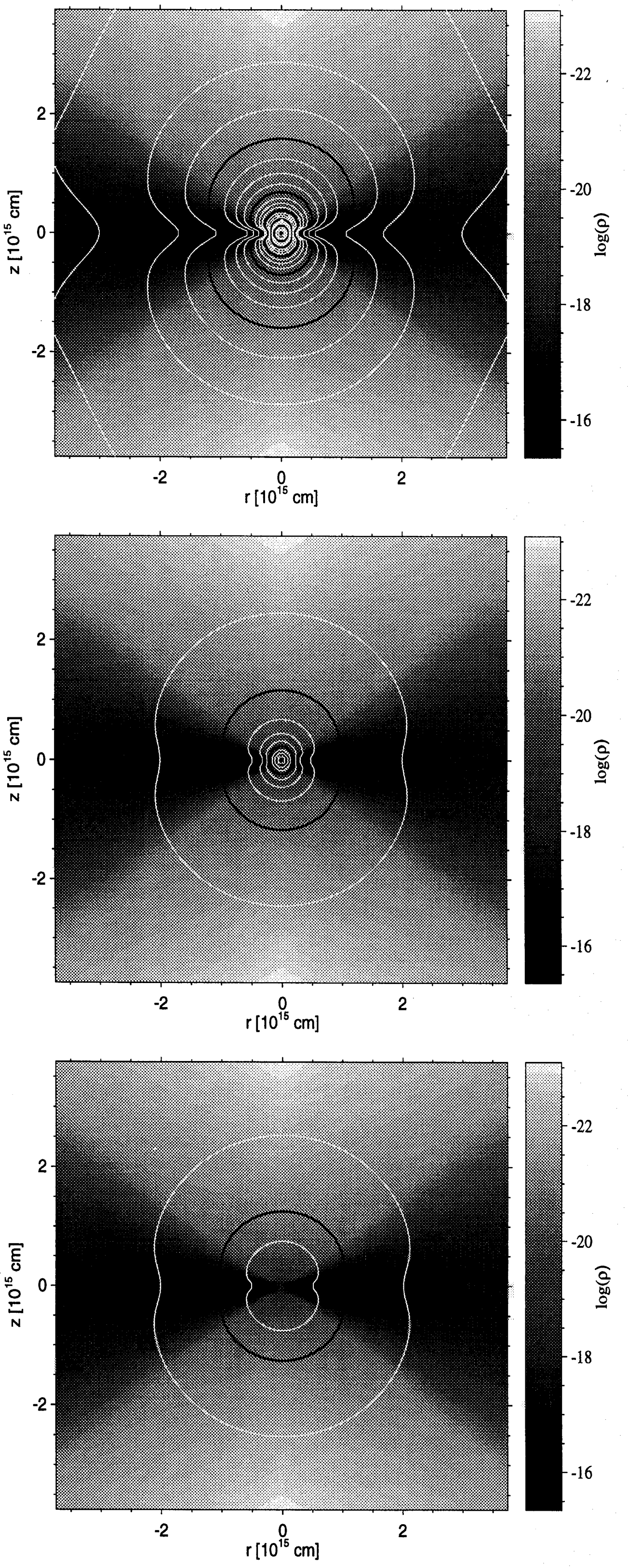

Fig. 3. Dust temperatures of model d5. The contour lines correspond to ΔT = 25 K, black lines to ΔT = 100 K. From the top: aC, silicate, ice-coated silicate. The outermost black contour lines are at 200 K, 100 K and 100 K, respectively

depths of the inner grid cells and thus to higher dust temperatures in the outer regions, because more short wavelength radiation can now escape from the center. We expect these differences to be much smaller in our model disk geometries, which do not have such a steep density gradient in the center.

In general the results of the two FLD codes are consistent and agree very well with the results of the exact program. It should be emphasized that our results are gained in a self consistent calculation and are therefore much more realistic than any of the widely used a priori power law approximations for the temperature distribution in a protostellar envelope. A comparison of the codes with equivalent grey versions can be found in Preibisch et al. (1994).

3.2. Dust temperatures

For a particular model, the temperature distributions of the three dust species are qualitatively similar. Figure 3 shows, as an example, the temperatures of carbon, silicate and ice-coated silicate grains in model d5. The density is displayed in the gray-scale background, the temperatures as contour lines at ΔT = 25 K. The 100 K, 200 K, ... lines are black. Ice-coatings exist only below 125 K; therefore the hottest innermost contour line of their temperature distribution corresponds to this value.

The carbon temperatures of the other models are displayed in Fig. 4. Very close to the central source their distributions have a spherical shape for all models. This changes in the outer region of the disk. The temperature in the disk is in general lower than around the axis at the same distance from the center. The deviation from the spherical shape is clearly correlated with the total optical depth of the disk. The isothermal slab, d4, which possesses the lowest and flattest density distribution of all models exhibits a nearly spherical temperature distribution, whereas the temperature in models d1 and d5 has a bone-like appearance. This dependence can also be seen from a comparison of the models with self-gravitating disks (d1, d2, d3) that only differ in the exponent of the radial decrease of the density.

3.3. Mean intensity J_ν

The mean intensity or zeroth moment J_ν is, as mentioned above, directly proportional to a more familiar quantity, the radiative energy density u_ν in the envelope. Its distribution is strongly frequency dependent, because of the strong dependence of the dust opacity on frequency (see Fig. 1).

As an example the spatial distribution of the zeroth moment at 156 μm, 25 μm and 350 nm of the models d1, d2, d3, d4 and d5 is shown in Fig. 5 (Note different gray-scale normalization). From the mm up to the far infrared range, the energy density in all models is approximately uniform, with a flat maximum in the central part of the disk component. From the far infrared to the near infrared an ellipsoidal distribution emerges. At lower frequencies it is elongated in the r-direction, i.e. the energy density in the disk region is still higher than perpendicular to it, whereas in the near infrared and optical range the energy density is higher in direction of the rotational axis than in the disk

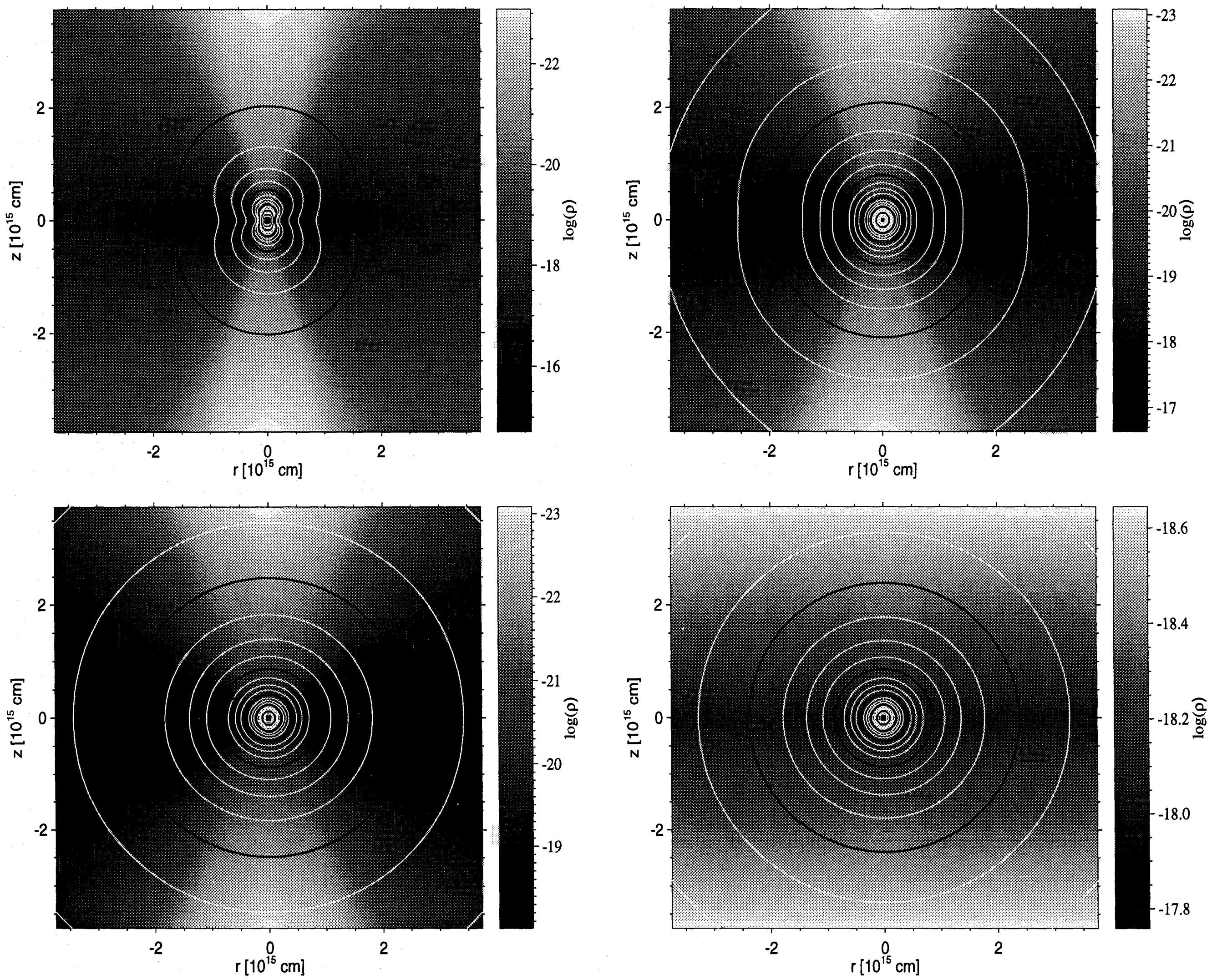

Fig. 4. aC temperatures: Contour lines as in Fig. 3. From upper left to lower right: d1, d2, d3 and d4. The outermost black lines mark 100 K, 200 K, 200 K and 200 K, respectively

at the same distance from the center. In the optical range, the models with very dense disks have a minimum in the equatorial region.

The main source of low frequency radiation is the emission of the cool dust in the envelope, but at these frequencies the envelope is optically thin. Both effects together produce a nearly uniform distribution with small maxima in high density regions.

The shorter the wavelength of the radiation the more its emission is confined to hot regions and the more effective it is absorbed in cooler parts. In a spherical envelope we would therefore expect a radial decrease of the energy density u_ν from the hot center outwards with a slope that becomes steeper with decreasing wavelength. In our model envelopes the gas density in the equatorial plane is much higher than perpendicular to it. The spatial distribution of the energy density in such an anisotropic configuration will in general deviate from the simple radial decrease expected in a spherical envelope. As a consequence of the differences between the frequency distribution of the energy density at two points, the same distance from the star, one lying near the equatorial plane and the other near the rotational axis, one can expect different dust temperatures at the two places. Thus, a highly non-isotropic and in some cases non-monotonic dust temperature distribution can result.

3.4. Spectra

From the known temperatures and zeroth moments, it is possible to calculate the spectral and spatial distribution of the flux emitted by a model object under a certain viewing angle. The spectra are mainly composed of two components: From the mm to mid infrared range the emission of the dust in the envelope dominates, whereas in the near infrared and optical regimes the partially absorbed and scattered radiation from the central source is most prominent. Certain features from the dust particles may also appear. The ice-coatings may cause an absorption

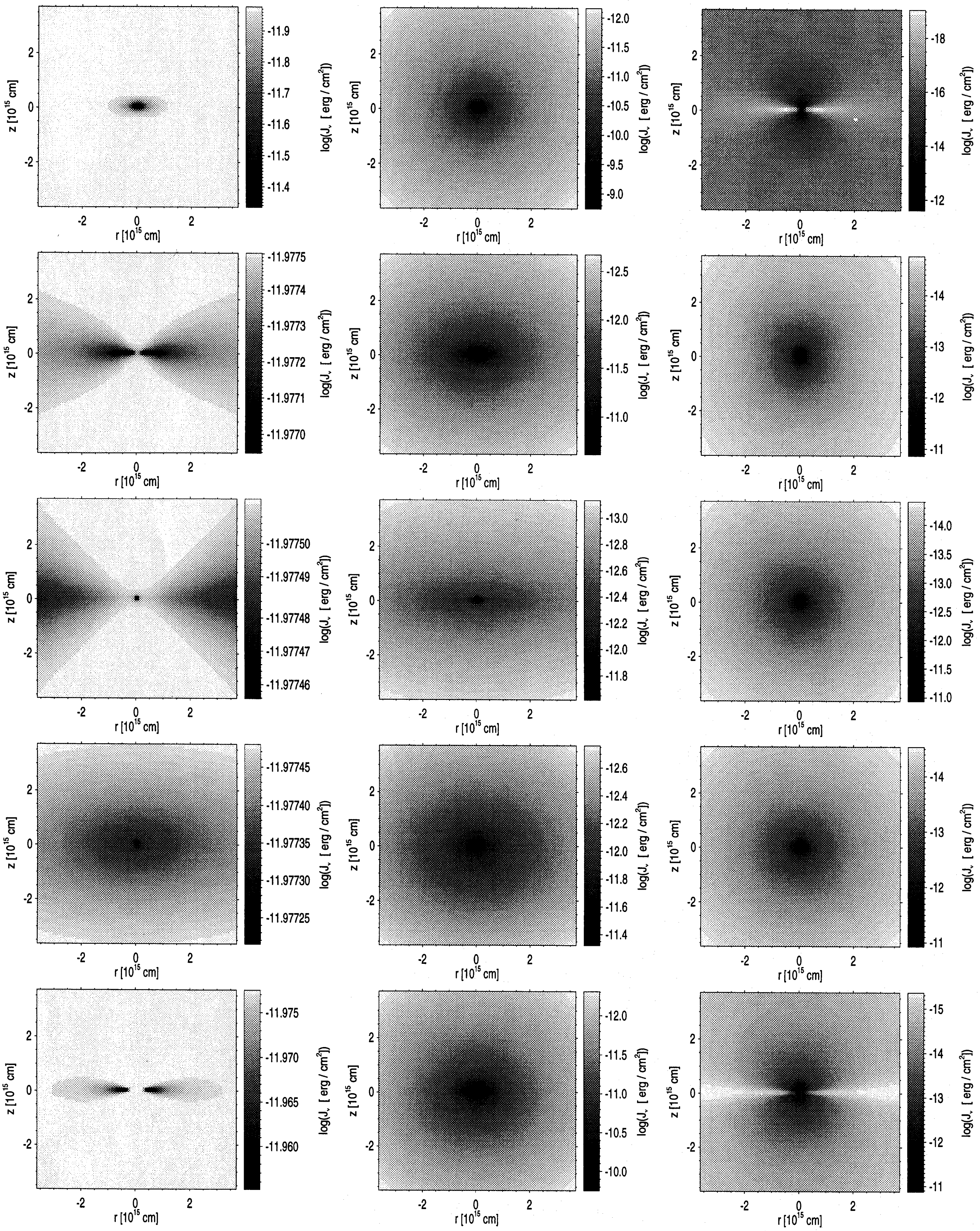

Fig. 5. From the top to the bottom: mean intensity of model d1 – d5 at 156 μm (left), 25 μm (middle) and 350 nm (right)

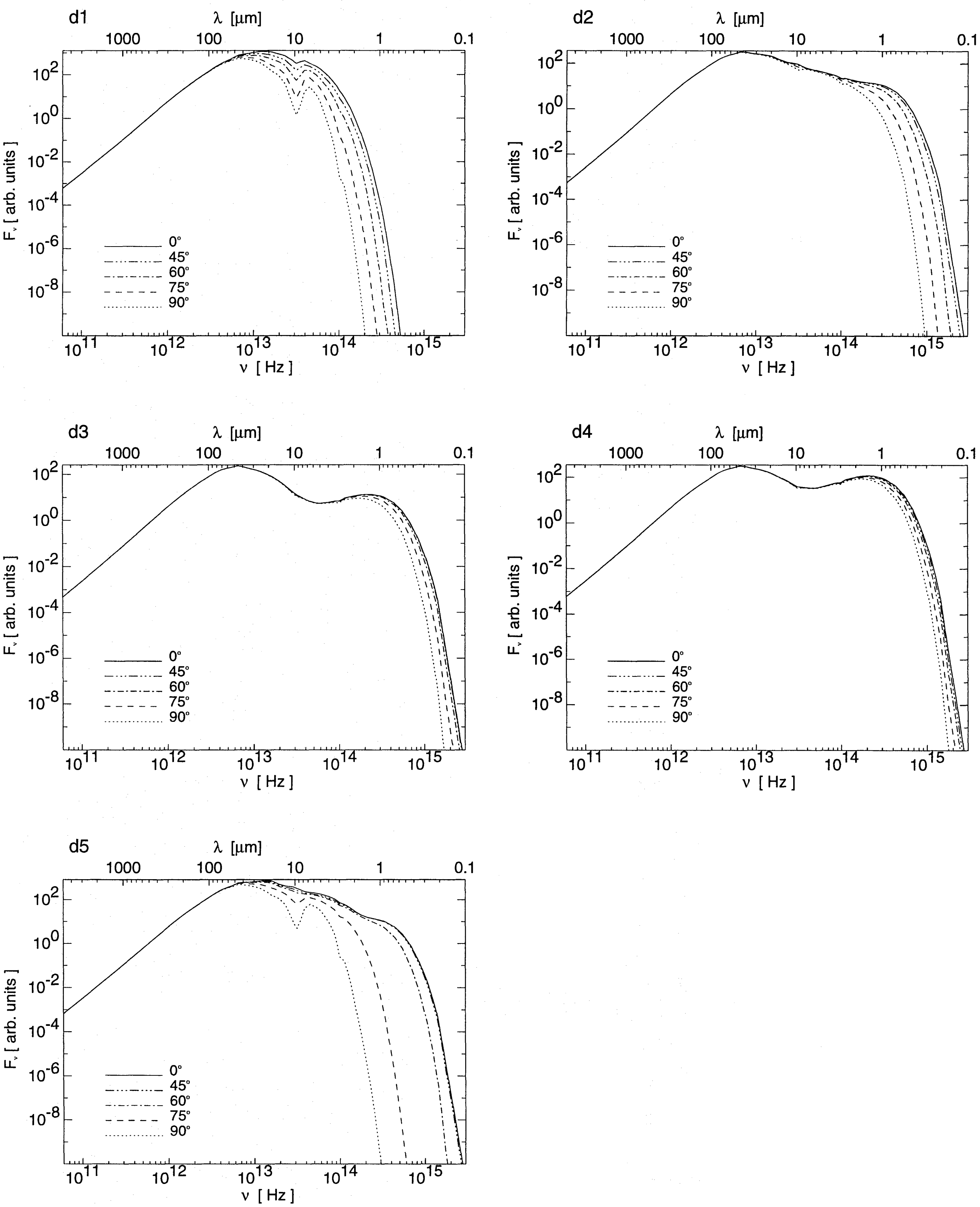

Fig. 6. From upper left to lower right: d1 – d5. Spectral distribution of the flux at different viewing angles

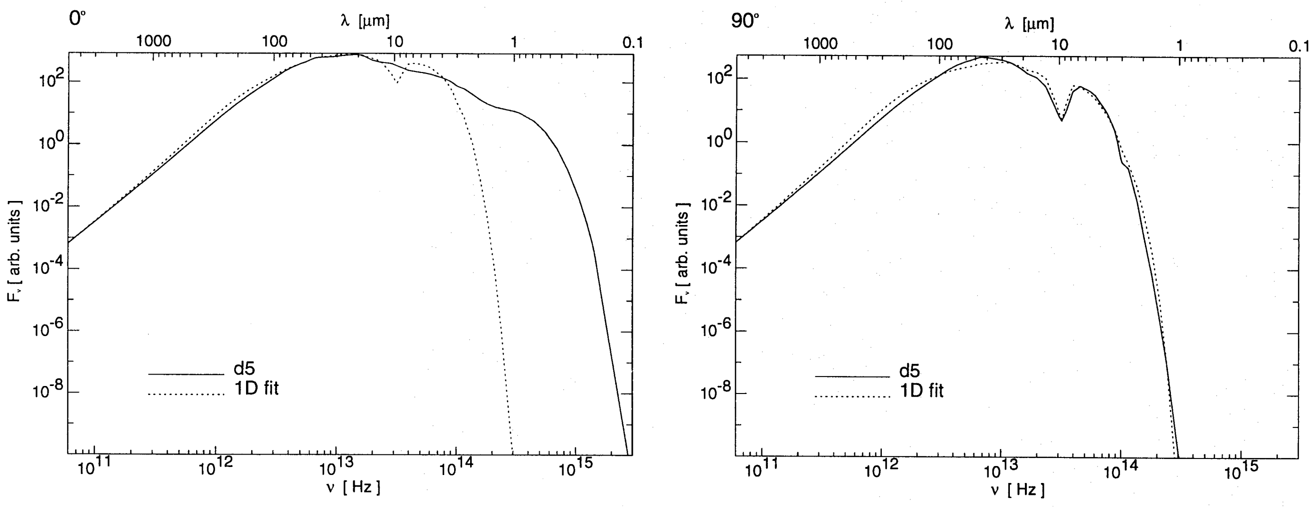

Fig. 7. 1D fits and the spectra of model d5 at 0° and 90°

feature at 3.1 μm and the silicate grains a feature at 10 μm, which can be seen either in absorption or in emission.

In Fig. 6 the spectra of the models at several viewing angles are shown. An angle of 90° corresponds to an edge-on view of the disk, 0° to a line of sight along the rotational axis. The spectra of all models change more or less with the viewing angle. Whereas the mm and far infrared part of the spectrum is nearly independent of the viewing angle (because the envelope is optically thin in this wavelength range and the flux therefore depends only on the total dust mass), the mid infrared and optical parts of the spectrum clearly show a variation with the inclination of the disk. The flux of all models decreases with increasing angle. But the features also change: Emission features decrease and may even change to absorption and absorption features become more prominent with growing viewing angle.

For example, at small angles the spectrum of the model with the Keplerian disk, d5, has a broad shape, which decreases slowly, almost monotonically from 20 μm to 500 nm except for a very small absorption feature from the ice at 3.1 μm and an emission feature from the silicate particles at about 10 μm. At an inclination above 60° the spectra look totally different. The flux at wavelength below about 3 μm is significantly diminished so that now the spectrum is more strongly peaked. The ice feature has grown and the silicate feature has changed from a weak emission feature to a strong absorption feature.

The spectrum that is observed in a certain direction depends on the opacity and temperature of the matter along the lines of sight. Therefore the models with dense disks, which also have the most anisotropic temperature distributions, show the greatest variations with the viewing angle in their spectral appearance.

For the density configurations considered here the radiation from the inner parts of the disk and from the central star itself is not significantly altered at small viewing angles by the low density material above the disk. With increasing angle the column densities of the central lines of sight increases. Thus, for non-negligible optical depth the short wavelength part of the spectrum nearly vanishes and the maximum of the dust emission is shifted to longer wavelengths.

The variation of the features is interesting, too. Whether the silicate feature is seen in emission or absorption depends on the temperature distribution along the line of sight. At 300 K the maximum of Planck's function is at about 10 μm. If warmer silicate particles dominate an emission feature results, if cooler silicate particles do, as in the models with steep temperature gradients (e.g. d1), a prominent absorption feature can be observed. If the gradient varies with direction a feature may even change from emission to absorption as in d5 and d2 depending on the viewing angle.

In addition, we have tested whether the spectra can be reproduced by spherical symmetric dusty envelope models. For this purpose we have tried to fit the spectra calculated from the disk model d5 with the code of Yorke (Yorke 1980b) that calculates an exact solution of the 1D radiation transfer. We have used power law density distributions $\rho(r) \propto r^{\alpha}$ that yield the same total mass of dust as the disk/envelope model. The dust model, the total mass of the envelope, the temperatures of the central source and the outer boundary were the same as in the disk/envelope model. We tried to fit the 2D spectrum by varying the exponent of the power law distribution, the radius of the envelope and the total luminosity. The 2D spectra for 0° and 90° are shown in Fig. 7 as solid lines.

The "best fit" spectra produced by the 1D model are given by dotted lines. The 2D spectrum for 90° can be reproduced rather well by a spectrum of a spherical symmetric envelope with α = 1.7 and with a total luminosity that is 770 times smaller than the total luminosity of the disk/envelope model. In contrast to this, the spectra for inclination angles less than 90° cannot reproduce the increased near infrared flux of the 2D spectra. We could only fit the spectrum up to 5 μm, by using α = 1.8, an outer radius of $10^{16.2}$ cm and a total luminosity that is 15 times smaller than the total luminosity of the disk/envelope model.

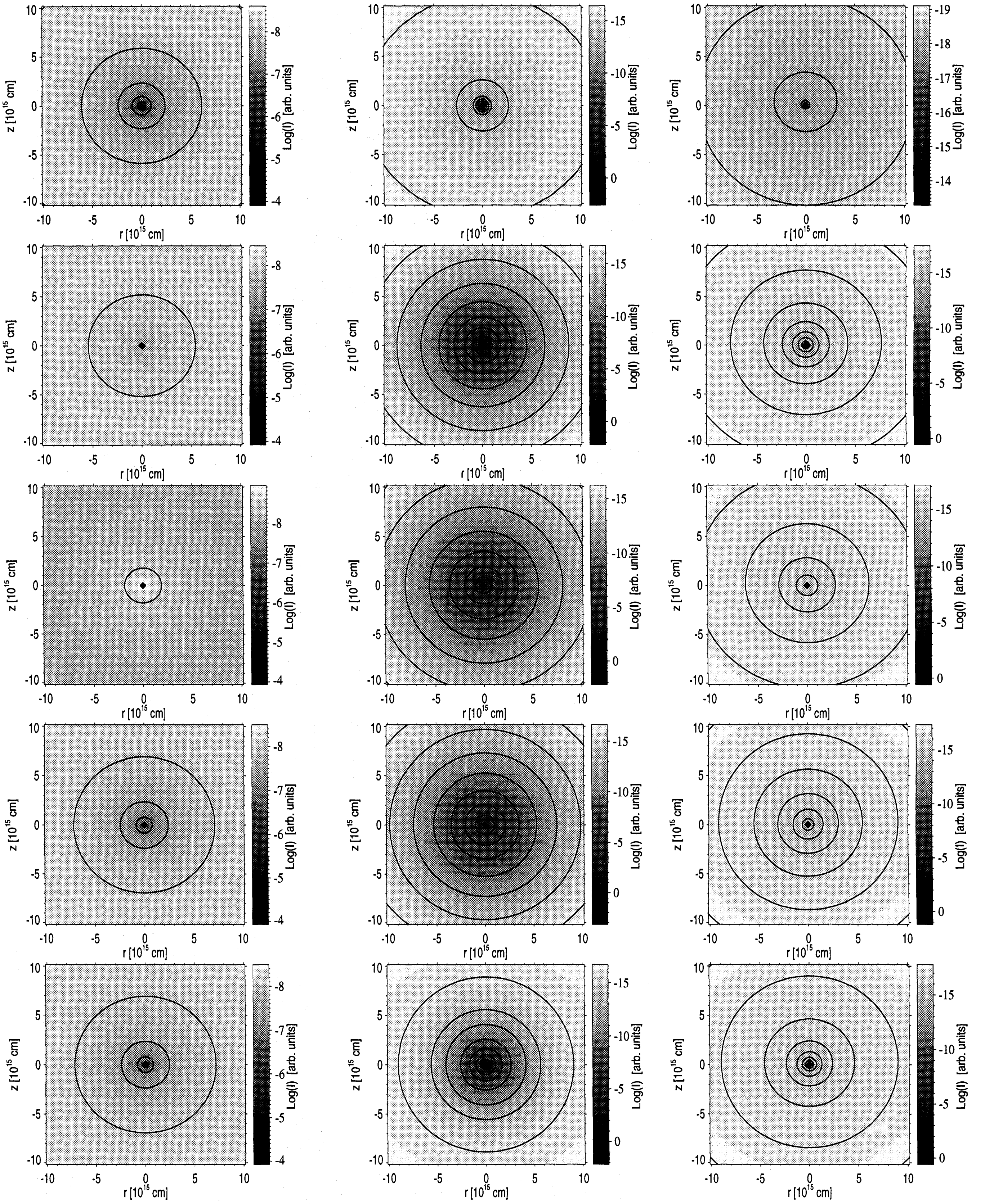

Fig. 8. From the top: d1 – d5. Intensity emitted at 5 mm (left), 3.45 μm (middle) and 350 nm (right) at a viewing angle of 15°. Δlog(I) of the contour lines is 0.5 (left), 2 (middle) and 0.5 (right)

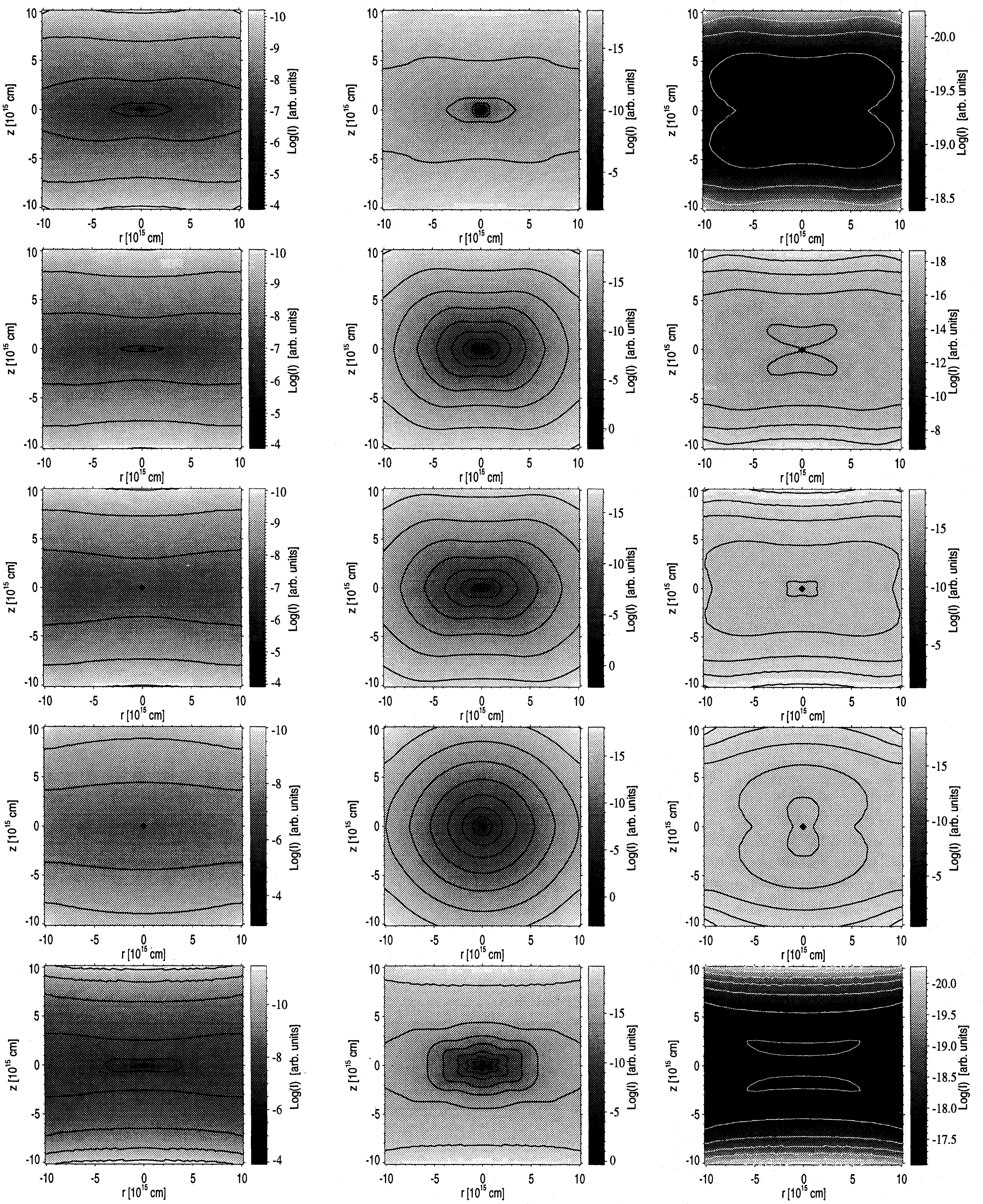

Fig. 9. From the top: d1 – d5. Intensity emitted at 5 mm (left), 3.45 μm (middle) and 350 nm (right) at a viewing angle of 90°. Δlog(I) of the contour lines is 1 (left), 2 (middle) and 0.5 (right)

Thus, if the submillimeter and far infrared flux can be fitted by a spherical model, an excess of the measured near infrared flux relative to the fit is a clear indication of the existence of a disk. But being able to find a spherically symmetric fit to the spectrum does not necessarily mean that the material is actually distributed in an almost spherical manner.

3.5. Intensity maps

In Figs. 8 and 9 the intensity distributions emitted from the five models at 5 mm, 3.45 μm and 350 nm at an inclination of 15° and 90° are shown as combined gray-scale and isophote maps.

At 5 mm the disks are optically thin and the 15° maps show, apart from the emission peak coming directly from the central source, a nearly uniform intensity that grows slowly towards the inner dense parts of the disks in models d1, d2, d4, and d5 and even decreases in d3. The differing map of d3 can be explained by the effect of the low density in the cavities and the destruction of the ice-coatings due to the high temperature, which both result in a smaller low frequency emission around the rotational axis. In the 90° figures the disks can nearly be seen at this frequency, because the isophotes follow closely the column density of the disks.

At 3.45 μm the intensity is determined by two effects: It grows with the temperatures in the envelopes as well as with the column density of a particular line of sight. Near and in the equatorial plane the temperature may be lower but the density is higher than near the axis at the same radius. Therefore the outward decrease of the intensity perpendicular to the disk has the same order of magnitude in the 90° maps and the models look less "disk-like" than at lower frequencies.

At 350 nm the dust is too cold for significant emission and in the 90° maps the equatorial regions are even obscured by the disk.

4. Conclusions and discussion

We have developed a method that allows us to simultaneously calculate dust temperatures and the frequency-dependent radiation energy density distribution in rotationally symmetric dusty circumstellar envelopes. By not using the gray approximation we show that in a disk-like configuration the spatial distributions of these quantities are highly non-spherically symmetric. Furthermore, the distribution of mean intensity is strongly frequency dependent. The properties of these internal physical quantities affect both the observable parameters of circumstellar envelopes and the disk's global evolution. Questions pertaining to the onset of instabilities, turbulent mixing processes, convection, the formation of planetesimals and the fate of material not collected into stars cannot be considered without intimate knowledge of the thermal properties of the material. For example, a nearly spherically symmetric temperature distribution leads to the conclusion that disks are not convectively unstable in the perpendicular direction (there is little dependence of temperature with height), whereas some of our models display rather large temperature gradients.

In a disk-like configuration the inclination of the disk is an essential parameter for modeling the source and inferring its evolutionary state. Non-detection of flux in the short wavelength range may not necessarily be indicative of a young deeply embedded source; it may also correspond to a more evolved object with an optically thick disk seen under a large inclination. Therefore it is essential to determine some of the properties of an object by other observations (e.g. composition of the dust and age or the inclination) before drawing conclusions regarding the evolutionary state from the spectrum of the source alone.

Our model intensity maps show that the intensity distribution in the millimeter range gives, at least at large inclinations, a good indication of the density distribution of the envelopes. High resolution mapping at several wavelengths combined with detailed radiation transfer modeling are necessary for an accurate determination of the distribution of material within the disk and in general a deeper understanding of protostellar systems with disks. However, such detailed information will not be available in the foreseeable future.In order to reduce the number of free parameters more realistic simulations of disk evolution would be useful.

Acknowledgements. We thank the Deutsche Forschungsgemeinschaft for financial support. Numerical calculations were conducted at the RZUW Würzburg

References

Beckwith, S., Sargent, A. 1993, in E. Levy & J. Lunine, eds, Protostars and Planets III, Arizona University Press, p. 521
Bodenheimer, P., Yorke, H.W., Różyczka, M., Tohline, J. 1990, ApJ 355, 651
Boss, A. 1987, in D. Hollenbach & H. Thronson, eds, Interstellar Processes, Reidel Publishing Company, Dordrecht
Efstathiou, A., Rowan-Robinson, M. 1990, MNRAS 245, 275
Fischer, O., Henning, Th., Yorke, H.W. 1994, A&A 284, 187
Lazareff, B., Pudritz, R., Monin, J.-L. 1990, ApJ 358, 170
Levermore, C., Pomraning, G. 1981, ApJ 248, 321
Marsal, D. 1976, Die numerische Lösung partieller Differentialgleichungen, Bibliographisches Institut
Mathis, J., Rumpl, W., Nordsieck, K. 1977, ApJ 217, 425
Okorokov, V., Shustov, B., Tutukov, A., Yorke, H.W. 1985, A&A 142, 441
Palla, F. 1993, in: Infrared Astronomy, Cambridge University Press
Preibisch, Th. 1992, Diplom-Thesis, Universität Würzburg
Preibisch, Th., Ossenkopf, V., Yorke, H.W., Henning, Th. 1993, A&A 279, 575
Preibisch, Th., Sonnhalter, C., Yorke, H.W. 1994, A&A (submitted)
Press, W.H., Flannery, B.P., Teukolsky, S.A., Vetterling, W.T. 1992, Numerical Recipes: The Art of Scientific Computing, 2. edn, Cambridge University Press
Shakura, N., Sunyaev, R. 1973, A&A 25, 337
Sonnhalter, C. 1993, Diplom-Thesis, Universität Würzburg
Strom, S., Edwards, S., Skrutzkie, M. 1993, in E. Levy & J. Lunine, eds, Protostars and Planets III, University of Arizona Press, p. 837
Tscharnuter, W., Boss, A. 1993, in E. Levy & J. Lunine, eds, Protostars and Planets III, p. 921
Yorke, H.W. 1979, A&A 80, 308
Yorke, H.W. 1980a, A&A 85, 215
Yorke, H.W. 1980b, A&A 86, 286
Yorke, H.W., Bodenheimer, P., Laughlin, G. 1993, ApJ 411, 274
Yorke, H.W., Kaisig, M. 1994, Comp. Phys. Comm. (in press)
Yorke, H.W. 1986, in K. Winkler & M.L. Norman, eds, Astrophysical Radiation Hydrodynamics, p. 141
Zinnecker, H., Bastien, P., Arcoragi, J.P., Yorke, H.W. 1992, A&A 265, 726